Journal of Power Sources 432 (2019) 1–7

Contents lists available at ScienceDirect

Journal of Power Sources

journal homepage: www.elsevier.com/locate/jpowsour

Development of Na_2FePO_4F/Conducting-Polymer composite as an exceptionally high performance cathode material for Na-ion batteries

Wonseok Ko [a], Jung-Keun Yoo [b], Hyunyoung Park [a], Yongseok Lee [a], Hyungsub Kim [c], Youngseok Oh [b], Seung-Taek Myung [a,*], Jongsoon Kim [a,**]

[a] Department of Nanotechnology and Advanced Materials Engineering, Sejong University, 209 Neungdong-ro, Gwangjin-gu, Seoul, Republic of Korea
[b] Carbon Composites Department, Composites Research Division, Korea Institute of Materials Science (KIMS), 797 Changwondaero, Changwon, Republic of Korea
[c] Korea Atomic Energy Research Institute (KAERI), Daedeok-daero 989 Beon-Gil, Yuseong-gu, Daejeon, Republic of Korea

HIGHLIGHTS

- PEDOT-coating.
- Outstanding rate-capability.
- 70% retention over 700 cycles.

GRAPHICAL ABSTRACT

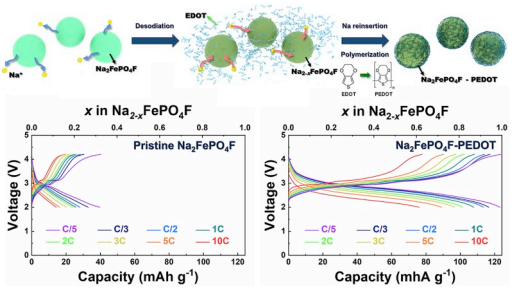

ARTICLE INFO

Keywords:
Na_2FePO_4F
Poly 3,4-ethylenedioxythiophene
Na-ion batteries
Advanced analysis
Cathode

ABSTRACT

Na_2FePO_4F encircled by a nanolayer composed of a conductive polymer, poly(3,4-ethylenedioxythiophene) (PEDOT), is prepared using a simple low-temperature process, and X-ray diffraction analysis indicates that the Na_2FePO_4F–PEDOT composite is the pure phase without any impurities. The existence and uniform encapsulation of PEDOT on the surface of the Na_2FePO_4F particles are clearly confirmed through Fourier-transform infrared spectroscopy and transmission electron microscopy. The PEDOT coating results in remarkably enhanced electrochemical performance compared with that of pristine Na_2FePO_4F. At C/5 (1C = 124 mA g^{-1}), the Na_2FePO_4F–PEDOT composite retains a specific capacity of ~123.1 mAh g^{-1}, which is close to its theoretical capacity. Even at 10C, the Na_2FePO_4F–PEDOT composite delivers a capacity of ~76.1 mAh g^{-1}, which is ~10 times higher than that of pristine Na_2FePO_4F under the same conditions. Furthermore, the Na_2FePO_4F–PEDOT composite maintains ~70% of its initial discharge capacity over 700 cycles at 1C.

1. Introduction

Environmental problems such as air pollution and the greenhouse effect have led to considerable efforts to develop eco-friendly vehicles such as electric vehicles (EVs). Although Li-ion batteries (LIBs) are extensively applied as energy storage systems (ESSs) for portable

* Corresponding author.
** Corresponding author.
E-mail addresses: smyung@sejong.ac.kr (S.-T. Myung), jongsoonkim@sejong.ac.kr (J. Kim).

https://doi.org/10.1016/j.jpowsour.2019.05.066
Received 23 March 2019; Received in revised form 10 May 2019; Accepted 17 May 2019

electronic devices such as cellphones and laptops because of their high energy/power density [1–4], the limited Li sources in the earth result in a high production cost for LIBs. Therefore, it is not sufficient to rely on LIBs alone to satisfy the ever-increasing demands for ESSs [5–8]. Na-ion batteries (NIBs) are considered attractive alternatives to LIBs because of the unlimited Na sources in the earth as well as their similar reaction mechanism to LIBs [7–20]. Various studies have focused on the development of NIBs, resulting in improved safety, power, and energy densities. Na_2FePO_4F has received attention as a promising cathode material for NIBs because of its low production cost resulting from the Fe-based redox reaction and its high operation voltage of ~3.0 V (*vs.* Na^+/Na) with structural stability induced by the existence of PO_4F polyanions in the structure [7,9,21–23]. However, its intrinsically low electronic conductivity results in poor power capability, which is considered the major obstacle preventing the widespread use of Na_2FePO_4F [5–10,24–28].

To improve the low conductivity of electrode materials, carbon coating by simple mechanical mixing with conductive carbon [29,30] or carbonization using an organic compound [7,31,32] has generally been performed. Carbonization using an organic compound is considered better than other carbon-coating methods to improve the electrochemical performance of electrode materials because this process results in a uniform carbon coating on the surface of the particles. However, these organic-based carbon coating processes can result in the formation of non-environmentally friendly contamination such as volatile organic compounds (VOCs), CO, and CO_2 [33,34]. To improve the power capability of Na_2FePO_4F without causing pollution, we attempted to envelop the particles of Na_2FePO_4F with a conducting polymer, poly(3, 4-ethylenedioxythiophene) (PEDOT). Conductive polymers are attractive alternatives to conductive carbon to improve not only the electrical conductivity but also the mechanical flexibility of electrodes or electrolytes for rechargeable batteries [35–42]. In addition, conducting polymers can be uniformly coated on the surface of materials using low-temperature processes, which can prevent the evolution of air-polluting gases, unlike carbonization, which uses organic compounds [33,34]. Recent reports support the ability of conducting polymers to improve the electrochemical performances of electrode materials for rechargeable batteries [33–37,40–44].

Herein, we demonstrated that Na_2FePO_4F can deliver outstanding electrochemical performance after homogeneous encapsulation of a nanolayer of PEDOT on the surface of the particles. The Na_2FePO_4F–PEDOT composite delivered a capacity of ~123.1 mAh g^{-1} at C/5 (1C = ~124.2 mA g^{-1}). Even at 10C, the specific capacity of Na_2FePO_4F–PEDOT was maintained up to ~76.1 mAh g^{-1}, which is ~10 times higher than that of pristine Na_2FePO_4F. Furthermore, Na_2FePO_4F–PEDOT exhibited excellent capacity retention of ~70% (vs. its initial capacity) over 700 cycles at 1C.

2. Results and discussion

Fig. 1 presents a schematic illustration of the fabrication process for the Na_2FePO_4F–PEDOT composite. We prepared the partially desodiated phase $Na_{2-x}FePO_4F$ using NO_2BF_4, which is a strong oxidizing agent with a high redox potential of NO_2/NO_2^+. These oxidized transition metal ions can accelerate the polymerization of the 3,4-ethylenedioxythiophene (EDOT) monomer for formation of the conductive PEDOT. Thus, EDOT monomers would be predominantly polymerized on the surface of the particles of the desodiated phase $Na_{2-x}FePO_4F$. Furthermore, persulfate was applied as the counter ion for the oxidized state of PEDOT, enabling the formation of a polymer with high conductivity [33,44]. After polymerization of EDOT to obtain the PEDOT coating, Na ions were re-inserted into the structure, and finally, we prepared the Na_2FePO_4F–PEDOT composite. To verify the structural change resulting from the PEDOT coating on the Na_2FePO_4F particles, X-ray diffraction (XRD) patterns of each sample were analyzed using Rietveld refinement. Supporting Fig. S1 presents the XRD patterns of pristine Na_2FePO_4F,

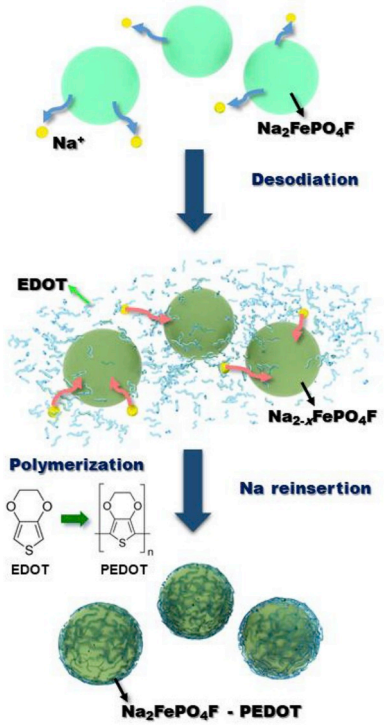

Fig. 1. Schematic illustration of the fabrication process for the Na_2FePO_4F–PEDOT composite. PEDOT was uniformly deposited on the surface of Na_2FePO_4F.

desodiated $Na_{2-x}FePO_4F$, and Na_2FePO_4F–PEDOT. No contamination or second phases were detected in any of the XRD patterns. The XRD pattern and lattice parameters of Na_2FePO_4F changed as a function of the Na content in the structure. As observed in Supporting Table T1, during desodiation, the *a* and *c* lattice parameters of Na_2FePO_4F decreased and the *b* lattice parameter increased. Inductively coupled plasma-atomic emission spectroscopy (ICP-AES) analysis revealed that ~0.3 Na ions were deintercalated from the structure by chemical desodiation. The XRD pattern of the Na_2FePO_4F–PEDOT composite in Fig. 2a shows that after polymerization, ~0.3 Na ions were re-inserted into the structure without any impurities. The lattice parameters of the Na_2FePO_4F–PEDOT composite with *Pbcn* symmetry were calculated to be $a = 5.2352(2)$ Å, $b = 13.8365(4)$ Å, and $c = 11.7728(3)$ Å, which agreewell with previously reported data [45]. Detailed structural information for the Na_2FePO_4F–PEDOT composite is provided in the Supporting Table T2. Full occupation of the Na sites was observed, which indicates that Na ions were successfully re-inserted into the structure. The atomic ratio of Na:Fe:P in the Na_2FePO_4F–PEDOT composite was confirmed to be 2:1:1 by ICP-AES analysis. Additionally, a bond–valence–sum (BVS) energy map was prepared for visualization of the possible Na diffusion paths using the Bond_Str program implemented in the FullProf package [46,47]. The Na_2FePO_4F framework is a layered-type structure, with each layer composed of a combination of bioctahedra $Fe_2O_6F_3$ and PO_4 tetrahedra. The bioctahedra $Fe_2O_6F_3$ units are formed through the face-sharing of two Fe-based octahedra, and the $Fe_2O_6F_3$ units are linked to each other via a F atom. The infinite chains of $Fe_2O_6F_3$ propagate along the *a*-axis, and each chain is connected with PO_4 tetrahedra in the *ac* plane. Na ions occupy the interlayer space between $[Fe_2O_6F_3– PO_4]_\infty$ chains. As shown in Fig. 2b, the Na ions in Na_2FePO_4F are interconnected in large two-dimensional (2D) diffusion paths within the *ac* plane, which indicates that Na_2FePO_4F can exhibit great power capability if its electronic conductivity is improved through the PEDOT coating.

The existence of PEDOT in the composite was confirmed by Fourier-transform infrared spectroscopy (FT-IR) analysis. Compared with

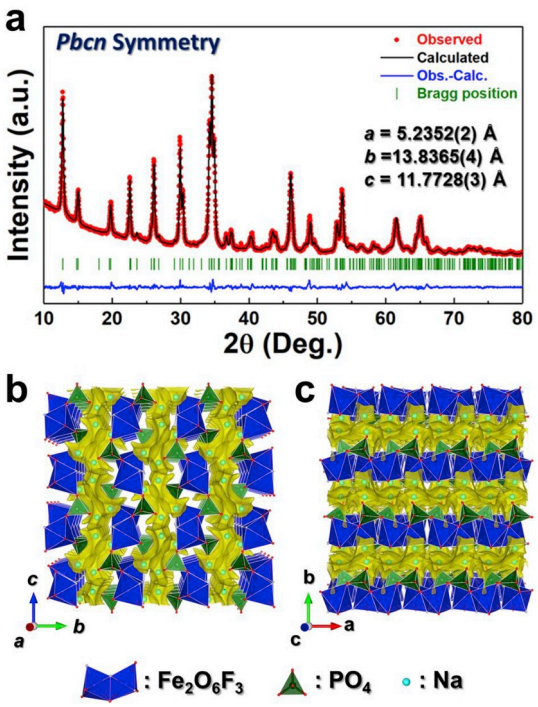

Fig. 2. (a) Refined XRD patterns of Na_2FePO_4F–PEDOT composite ($R_P = 5.39\%$, $R_I = 6.92\%$, $R_F = 6.36\%$, and $\chi^2 = 8.14\%$) and BVS energy maps of Na_2FePO_4F in (b) *bc* plane and (c) *ab* plane.

pristine Na_2FePO_4F, additional vibrations were observed for the Na_2FePO_4F–PEDOT composite, including C=C ring and C–O–R vibrations at 1183 and 1114 cm^{-1}, respectively; C–S vibration at 943 cm^{-1}; polymer *p*-doping band vibration at 1320 cm^{-1}; and vibration by ring stretching of thiophene ring at 1520 cm^{-1} as well as vibrations by PO_4 tetrahedra (508 and 630 cm^{-1} for O–P–O bonds and 1010–1197 cm^{-1} for ν_{as} of P–O bonds in PO_3) (Supporting Fig. S2). These findings indicate the successful formation of PEDOT in the composite. Furthermore, the high-resolution transmission electron microscopy (HRTEM) images in Fig. 3a and b clearly show that the primary particles with sizes of ~200 nm were completely coated by an amorphous layer of 5-nm thickness. Energy-dispersive X-ray spectroscopy (EDS) analysis confirmed that the amorphous layer was PEDOT containing sulfur (S) atoms in the structure, as shown in Fig. 3c and d. Additionally, as observed in Fig. 3e, elemental line-scan analyses revealed that less Fe and P than S appeared at the edges of the particles. These results are indicative of successful PEDOT coating on the surface of the Na_2FePO_4F particles. The weight percentage of PEDOT in the Na_2FePO_4F–PEDOT composite was measured using thermogravimetric analysis (TGA). The difference in the weight loss between the pristine Na_2FePO_4F and Na_2FePO_4F–PEDOT composite was ~6%, which corresponds to the amount of PEDOT in the composite (Supporting Fig. S3). Moreover, as shown in Supporting Fig. S4, electrochemical impedance spectroscopy (EIS) revealed that the charge-transfer resistance of Na_2FePO_4F–PEDOT was much lower than that of pristine Na_2FePO_4F, which indicates that the presence of the conductive polymer (PEDOT) plays an important role in improving the electrical conductivity of Na_2FePO_4F. The effect of the PEDOT coating on Na_2FePO_4F was confirmed by electrochemical measurements, which were compared with those for a pristine Na_2FePO_4F electrode using an equivalent weight of conductive carbon (6 wt%) instead of PEDOT. The power capabilities of the two samples were tested under various current rates (C/5, C/3, C/2, 1C, 2C, 3C, 5C, and 10C) from 4.2 to 2.0 V. As observed in Fig. 4a, the Na_2FePO_4F–PEDOT composite delivered exceedingly higher capacities than pristine Na_2FePO_4F at all the current rates. The discharge capacity and the charge capacity of the Na_2FePO_4F–PEDOT composite at C/5 was ~123.1 mAh g^{-1} and ~123.6 mAh g^{-1}, which is close to the theoretical capacity of Na_2FePO_4F. The discharge capacity of Na_2FePO_4F–PEDOT at 10C was ~10 times higher than that of pristine Na_2FePO_4F (Fig. 4b). We performed further electrochemical test to verify the specific capacity of pristine Na_2FePO_4F at the low current rate such as C/10, C/20 and C/50. As shown in Supporting Fig. S5, at C/50, the pristine Na_2FePO_4F delivers the specific capacity of ~100 mAh g^{-1}. Furthermore, comparison of the cycle performances of pristine Na_2FePO_4F and the Na_2FePO_4F–PEDOT composite (Supporting Fig. S6) reveals that the Na_2FePO_4F–PEDOT composite exhibited remarkably enhanced cyclability. As observed in Fig. 4c and d, the Na_2FePO_4F–PEDOT composite maintained up to ~70% of its initial discharge capacity over 700 cycles with a high coulombic efficiency of more than 98.5%.

To verify the structural change of the Na_2FePO_4F–PEDOT composite during the charge/discharge process, we performed *ex situ* XRD analysis on $Na_{2-x}FePO_4F$–PEDOT samples with various Na contents. In

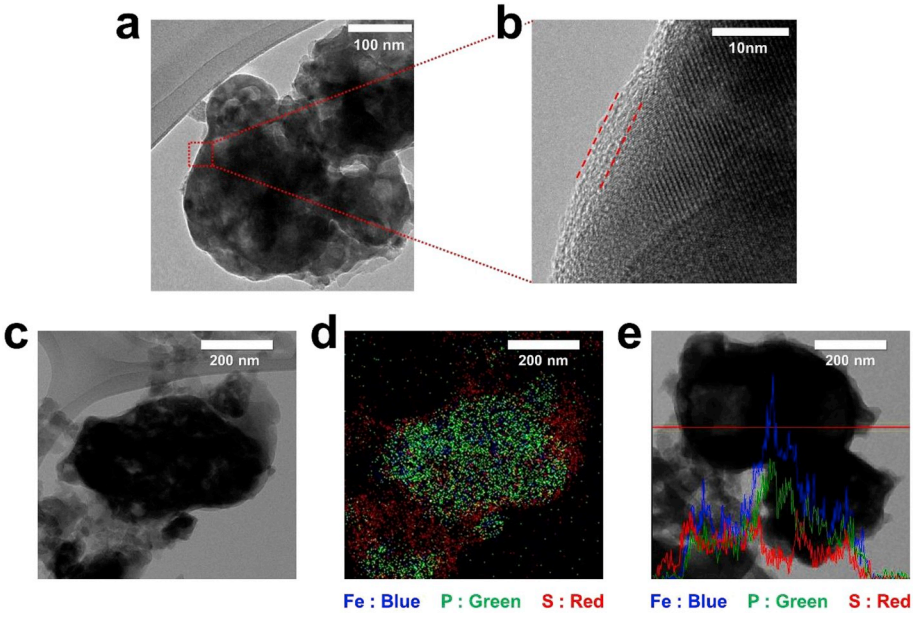

Fig. 3. (a) ~ (b): HRTEM image of (a) Na_2FePO_4F–PEDOT composite and (b) enlargement of boxed area in (a). (c) ~ (e): STEM analyses in (c) bright-field mode, (d) elemental analysis using EDX mapping (Fe: blue, P: green, S: red) of Na_2FePO_4F–PEDOT composite, and (e) cross-sectional composition line profiles (V: blue, P: green, S: red) of Na_2FePO_4F–PEDOT composite. (For interpretation of the references to color in this figure legend, the reader is referred to the Web version of this article.)

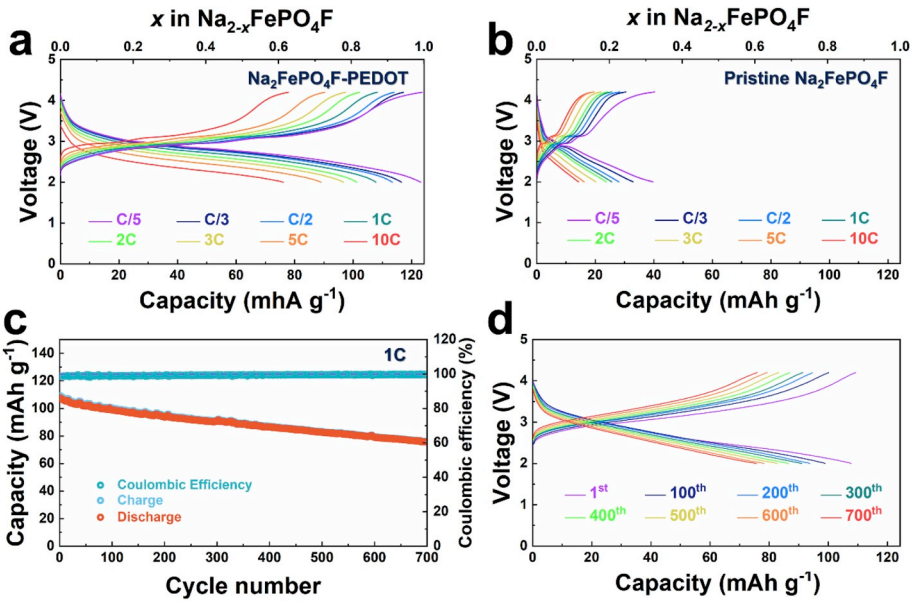

Fig. 4. (a) Specific discharge capacity of Na_2FePO_4F–PEDOT composite and (b) pristine Na_2FePO_4F in the voltage range of 2.0–4.2 V for various current rates (C/5, C/3, C/2, 1C, 2C, 3C, 5C, and 10C). (c) ~ (d) Specific charge/discharge capacity and coulombic efficiency of Na_2FePO_4F–PEDOT at 1C (1C = ~124 mA g^{-1}).

Supporting Fig. S7, it was showed Na deintercalation curve of $Na_{2-x}FePO_4F$-PEDOT ($0 \leq x \leq 0.99$), and the overall XRD pattern of $Na_{2-x}FePO_4F$–PEDOT (Fig. 5a) verified the change of structure when Na deintercalated from the structure. In particular, the intensities of some XRD peaks, such as 020, 002, 022, 102, and 023, significantly changed, and their 2θ positions shifted. Through X-ray absorption near-edge structure (XANES) analyses, it was verified that the Fe oxidation state of $Na_{2-x}FePO_4F$–PEDOT continuously changed between +2 and + 3 as a function of Na content (Fig. 5b), which indicates that all the $Na_{2-x}FePO_4F$–PEDOT samples for the *ex situ* XRD analyses were successfully prepared. In addition, we determined the volume and lattice parameters of the $Na_{2-x}FePO_4F$–PEDOT samples using Rietveld refinement [48]. As observed in Fig. 6, the total volume change of Na_2FePO_4F during the charge/discharge process was ~4.70%, which is relatively larger than that of other cathode materials with outstanding cycle performance [22, 49]. Thus, we supposed that the capacity fading of Na_2FePO_4F-PEDOT composite may mainly result from the repeated volume expansion/-shrinkage of Na2FePO4F phase over 700 cycles. As shown in Supporting Fig. S8, the morphology of Na_2FePO_4F-PEDOT electrode was very similar both before and after cycling for 700 cycles (S7a and S7b). Furthermore, XRD patterns (S7c) were almost same despite large volume change during cycling. We speculate that the particular modification of Na_2FePO_4F using the PEDOT coating results in the outstanding cycle performance of the Na_2FePO_4F–PEDOT composite (comparable to that reported for other NIB electrode materials with surface coatings) despite its large volume change during the charge/discharge process [48].

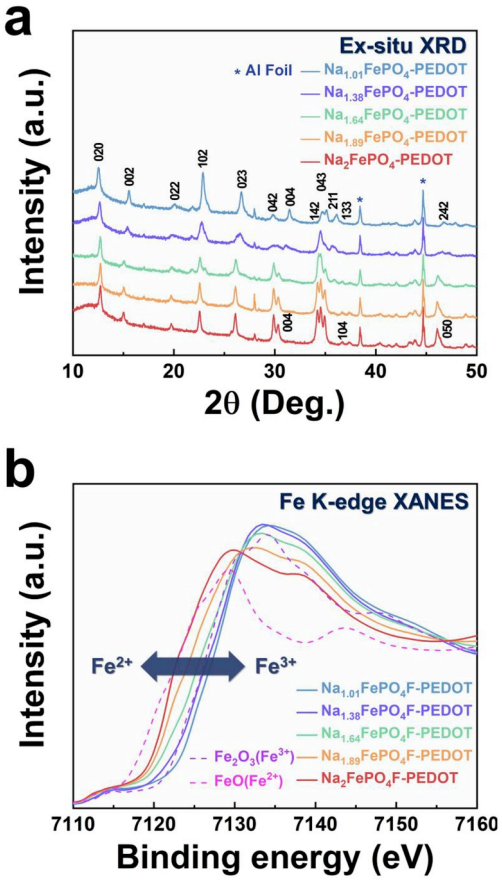

Fig. 5. (a) *Ex situ* XRD patterns of $Na_{2-x}FePO_4F$–PEDOT ($0 \leq x \leq 0.99$). (b) Fe K-edge XANES spectra of $Na_{2-x}FePO_4F$–PEDOT ($0 \leq x \leq 0.99$).

3. Conclusions

In summary, we successfully prepared a Na_2FePO_4F–PEDOT composite with high power capability for use in NIBs using a simple and low-temperature process. During the PEDOT-coating process, no irreversible reactions occurred. In addition, XRD analysis with Rietveld refinement confirmed that the Na_2FePO_4F–PEDOT composite was a pure phase without any impurities. The homogeneous PEDOT coating was verified using FT-IR and TEM analyses and resulted in highly enhanced electrochemical performance of Na_2FePO_4F. The discharge capacity of the Na_2FePO_4F–PEDOT composite measured at C/5 was ~123.1 mAh g^{-1}, corresponding to its theoretical capacity. Even at 10C, the Na_2FePO_4F–PEDOT composite delivered a capacity of ~76.1 mAh g^{-1}, which is ~10 times higher than that of pristine Na_2FePO_4F. Furthermore, the PEDOT coating resulted in significantly enhanced cycle performance of Na_2FePO_4F, with ~70% retention of its initial capacity over 700 cycles at 1C. This study provides insight into possible methods to improve the

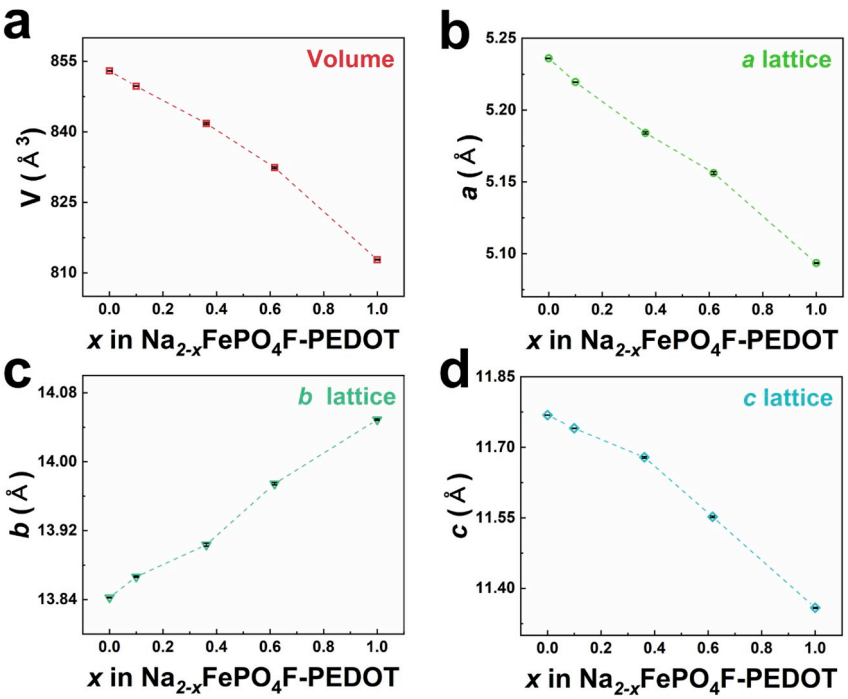

Fig. 6. Change in (a) volume and (b) *a*, (c) *b* and (d) *c* lattice parameters of $Na_{2-x}FePO_4F$–PEDOT ($0 \leq x \leq 0.99$) samples (error bars, black).

electrochemical performance of electrode materials for not only NIBs but also other rechargeable batteries.

4. Experimental section

4.1. Synthesis of Na_2FePO_4F

Na_2FePO_4F powder was synthesized using conventional solid-state synthesis. NaF (Alfa Aesar, 99%), Na_2CO_3 (Sigma Aldrich, 99.5%), $FeC_2O_4{\blacksquare}2H_2O$ (Sigma Aldrich, 99%), and $NH_4H_2PO_4$ (Sigma Aldrich, 98%) with a molar ratio of 1:0.5:1:1 were used as precursors. The precursors were mixed using high-energy ball-milling at 500 rpm for 12 h. After ball-milling, the mixture was finely ground and calcined at 350 °C under Ar + 5 wt% H_2 conditions for 5 h. After pre-heating, the powder was re-ground and calcined again at 600 °C under Ar + 5 wt% H_2 conditions for 10 h.

4.2. Preparation of $Na_{2-x}FePO_4F$

To prepare the $Na_{2-x}FePO_4F$ samples, the synthesized Na_2FePO_4F was chemically desodiation by NO_2BF_4 (Aldrich, 95%) according to the following reaction:

$$Na_2FePO_4F + xNO_2BF_4 \rightarrow Na_{2-x}FePO_4F + xNaBF_4 + xNO_2.$$

NO_2BF_4 is a strong oxidizing agent with a high redox potential of NO_2^+/NO_2 at ~4.8 V *vs.* Na^+/Na. The composition of $Na_{2-x}FePO_4F$ was controlled by adjusting the time of the reaction between the Na_2FePO_4F and NO_2BF_4 with a molar ratio of 1:0.3 in acetonitrile (Aldrich, 98%) at 60 °C in an Ar-filled glove box. The final product was transferred to a filter and rinsed with acetonitrile.

4.3. Preparation of Na_2FePO_4F–PEDOT

Sodium persulfate (1 g), EDOT (0.4 ml, Aldrich), and $Na_{2-x}FePO_4F$ (0.5 g) were added to ethanol (12 ml) and sealed [50]. This solution was stirred at 35 °C for 1 day. After 1 day, the color of the mixture turned slightly blue. The mixture was transferred to a filter and rinsed several times with ethanol and acetonitrile. The Na_2FePO_4F–PEDOT was dried at 80 °C overnight in a vacuum oven. To prepare the fully sodiated Na_2FePO_4F phase, we performed additional sodiation using NaI under argon reflux. To discover the optimal condition for preparation of Na_2FePO_4F-PEDOT composite, we performed various experiments with changing the mass ratio between EDOT and $Na_{2-x}FePO_4F$. When the amount of EDOT per 0.5 g $Na_{2-x}FePO_4F$ was decreased to 0.3 ml, we could not detect any signals on PEDOT in the FT-IR results, which indicates that the polymerization from EDOT to PEDOT was not occurred at the condition of 0.3 ml EDOT/0.5 g $Na_{2-x}FePO_4F$ (Supporting Fig. S9a). Furthermore, when the amount of EDOT per 0.5 g $Na_{2-x}FePO_4F$ was increased to 0.5 ml, despite successful polymerization of PEDOT (Supporting Fig. S9a), the crystal structure of Na_2FePO_4F was damaged, and then, it was transformed into an unknown crystal structure (Supporting Fig. S9b). Thus, we supposed that the condition of 0.4 ml EDOT/0.5 g $Na_{2-x}FePO_4F$ is optimal for preparation of $Na_{2-x}FePO_4F$-PEDOT composite.

4.4. Materials preparation

XRD patterns for the Na_2FePO_4F–PEDOT composite were obtained using an X-ray diffractometer (PANalytical) equipped with Cu-Kα radiation ($\lambda = 1.5406$ Å). The XRD measurements were performed over the 2θ range of 10°–80° with a step size of 0.01°. Each step was exposed for 4 s. Structural refinements were performed using the Rietveld method and FullProf software. The morphology and particle size parameters were analyzed using field-emission transmission electron microscopy (FETEM, PHILIPS Tecnai F20) operating at 200 kV. The samples were further characterized using Fourier-transform infrared (FT-IR) spectroscopy (JASCO) using KBr pellet analysis. The atomic ratios of elements such as Na, Fe, and P were determined using inductively coupled plasma atomic emission spectroscopy (ICP-AES; Thermo Jarrel Ash, Polyscan 60E, USA).

4.5. Electrochemistry

A slurry of 80 wt% Na_2FePO_4F–PEDOT composite (74 wt% Na_2FePO_4F and 6 wt% PEDOT), 10 wt% Super P, and 10 wt% polyvinylidene fluoride (PVDF) dispersed in N-methy1-2-pyrrolidone (NMP) was prepared and cast on aluminium foil. NMP was evaporated at 70 °C for 2 h.

The composition of the pristine Na_2FePO_4F electrode was 74 wt% Na_2FePO_4F, 16 wt% carbon, and 10 wt% PVDF. The fabrication process for the pristine Na_2FePO_4F electrode was the same as that for the Na_2FePO_4F–PEDOT composite. Electrochemical tests were performed using CR2032-type coin cells assembled in an Ar-filled glovebox. The mass loading of the active material on the working electrode was ~2 mg cm^{-2}. The cell was assembled using a Na counter electrode, a separator (GF/F glass fiber), and a 1 M solution of $NaPF_6$ in ethyl carbonate/propylene carbonate (EC/PC, 1:1 v/v) in an Ar-filled glove box. The electrochemical cells were assembled under an atmosphere of highly pure argon in a glove box. The charge/discharge tests were performed using a galvanostat (WonA Tech). 1C corresponds to ~124 mA g^{-1}.

Acknowledgements

This work was supported by Research Fund (PNK6080) of Korea Institute of Materials Science (KIMS).

Appendix A. Supplementary data

Supplementary data to this article can be found online at https://doi.org/10.1016/j.jpowsour.2019.05.066.

References

[1] M. Armand, J.M. Tarascon, Building better batteries, Nature 451 (2008) 652–657. https://doi.org/10.1038/451652a.
[2] J.M. Tarascon, M. Armand, Issues and challenges facing rechargeable lithium batteries, Nature 414 (2001) 359–367. https://doi.org/10.1038/35104644.
[3] K. Kang, Y.S. Meng, J. Breger, C.P. Grey, G. Ceder, Electrodes with high power and high capacity for rechargeable lithium batteries, Science 311 (2006) 977–980. https://doi.org/10.1126/science.1122152.
[4] J. Kim, D.H. Seo, S.W. Kim, Y.U. Park, K. Kang, Mn based olivine electrode material with high power and energy, Chem. Commun. 46 (2010) 1305–1307. https://doi.org/10.1039/b922133f.
[5] S.W. Kim, D.H. Seo, X.H. Ma, G. Ceder, K. Kang, Electrode materials for rechargeable sodium-ion batteries: potential alternatives to current lithium-ion batteries, Adv. Energy Mater. 2 (2012) 710–721. https://doi.org/10.1002/aenm.201200026.
[6] R.A. Shakoor, D.H. Seo, H. Kim, Y.U. Park, J. Kim, S.W. Kim, H. Gwon, S. Lee, K. Kang, A combined first principles and experimental study on Na3V2(PO4)(2)F-3 for rechargeable Na batteries, J. Mater. Chem. 22 (2012) 20535–20541. https://doi.org/10.1039/c2jm33862a.
[7] Y. Kawabe, N. Yabuuchi, M. Kajiyama, N. Fukuhara, T. Inamasu, R. Okuyama, I. Nakai, S. Komaba, Synthesis and electrode performance of carbon coated Na2FePO4F for rechargeable Na batteries, Electrochem. Commun. 13 (2011) 1225–1228. https://doi.org/10.1016/j.elecom.2011.08.038.
[8] N. Yabuuchi, M. Kajiyama, J. Iwatate, H. Nishikawa, S. Hitomi, R. Okuyama, R. Usui, Y. Yamada, S. Komaba, P2-type Na-x Fe1/2Mn1/2 O-2 made from earth-abundant elements for rechargeable Na batteries, Nat. Mater. 11 (2012) 512–517. https://doi.org/10.1038/nmat3309.
[9] Y. Kawabe, N. Yabuuchi, M. Kajiyama, N. Fukuhara, T. Inamasu, R. Okuyama, I. Nakai, S. Komaba, A comparison of crystal structures and electrode performance between Na2FePO4F and Na2Fe0.5Mn0.5PO4F synthesized by solid-state method for rechargeable Na-ion batteries, Electrochemistry 80 (2012) 80–84. https://doi.org/10.5796/electrochemistry.80.80.
[10] X.H. Zhang, W.L. Pang, F. Wan, J.Z. Guo, H.Y. Lu, J.Y. Li, Y.M. Xing, J.P. Zhang, X. L. Wu, P2-Na2/3Ni1/3Mn5/9Al1/9O2 microparticles as superior cathode material for sodium-ion batteries: enhanced properties and mechanisam via graphene connection, ACS Appl. Mater. Interfaces 8 (2016) 20650–20659. https://doi.org/10.1021/acsami.6b03944.
[11] Y.B. Shen, S. Birgisson, B.B. Iversen, A. P2-NaxCo0, 7Mn0.3O2 (x approximate to 1.0) cathode material for Na-ion batteries with superior rate and cycle capability, J. Mater. Chem. 4 (2016) 12281–12288. https://doi.org/10.1039/c6ta03630a.
[12] J. Kim, I. Park, H. Kim, K.Y. Park, Y.U. Park, K. Kang, Tailoring a new 4V-class cathode material for Na-ion batteries, Adv. Energy Mater. 6 (2016) 1502147. https://doi.org/10.1002/aenm.201502147.
[13] M. Huon Han, E. Gonzalo, N. Sharma, J. Miguel Lopez del Amo, M. Armand, M. Avdeev, J.J. Saiz Garitaonandia, T. Rojo, High-performance P2-phase Na2/3Mn0.8Fe0.1Ti0.1O2 cathode material for ambient-temperature sodium-ion batteries, Chem. Mater. 28 (2016) 106–116. https://doi.org/10.1021/acs.chemmater.5b03276.
[14] B. Fu, X. Zhou, Y. Wang, High-rate performance electrospun Na0.44MnO2 nanofibers as cathode material for sodium-ion batteries, J. Power Sources 310 (2016) 102–108. https://doi.org/10.1016/j.jpowsour.2016.01.101.
[15] Y. Wang, J. Liu, B. Lee, R. Qiao, Z. Yang, S. Xu, X. Yu, L. Gu, Y.-S. Hu, W. Yang, K. Kang, H. Li, X.-Q. Yang, L. Chen, X. Huang, Ti-substituted tunnel-type Na0.44MnO2 oxide as a negative electrode for aqueous sodium-ion batteries, Nat. Commun. 6 (2015). https://doi.org/10.1038/ncomms7401.
[16] H. Wang, D. Jiang, Y. Zhang, G. Li, X. Lan, H. Zhong, Z. Zhang, Y. Jiang, Self-combustion synthesis of Na3V2(PO4)(3) nanoparticles coated with carbon shell as cathode materials for sodium-ion batteries, Electrochim. Acta 155 (2015) 23–28. https://doi.org/10.1016/j.electacta.2014.12.160.
[17] J. Mao, C. Luo, T. Gao, X. Fan, C. Wang, Scalable synthesis of Na3V2(PO4)(3)/C porous hollow spheres as a cathode for Na-ion batteries, J. Mater. Chem. 3 (2015) 10378–10385. https://doi.org/10.1039/c5ta01007a.
[18] Y. Liu, Y. Qiao, W. Zhang, Z. Li, X. Ji, L. Miao, L. Yuan, X. Hu, Y. Huang, Sodium storage in Na-rich NaxFeFe (CN)(6) nanocubes, Nanomater. Energy 12 (2015) 386–393. https://doi.org/10.1016/j.nanoen.2015.01.012.
[19] Z. Hu, Z. Zhu, F. Cheng, K. Zhang, J. Wang, C. Chen, J. Chen, Pyrite FeS2 for high-rate and long-life rechargeable sodium batteries, Energy Environ. Sci. 8 (2015) 1309–1316. https://doi.org/10.1039/c4ee03759f.
[20] Q. An, F. Xiong, Q. Wei, J. Sheng, L. He, D. Ma, Y. Yao, L. Mai, Nanoflake-assembled hierarchical Na3V2(PO4)(3)/C microflowers: superior Li storage performance and insertion/extraction mechanism, Adv. Energy Mater. 5 (2015) 1401963. https://doi.org/10.1002/aenm.201401963.
[21] N. Recham, J.-N. Chotard, L. Dupont, K. Djellab, M. Armand, J.-M. Tarasconz, Ionothermal synthesis of sodium-based fluorophosphate cathode materials, J. Electrochem. Soc. 156 (2009) A993–A999. https://doi.org/10.1149/1.3236480.
[22] J. Kim, G. Yoon, M.H. Lee, H. Kim, S. Lee, K. Kang, New 4V-class and zero-strain cathode material for Na-ion batteries, Chem. Mater. 29 (2017) 7826–7832. https://doi.org/10.1021/acs.chemmater.7b02477.
[23] R. Tripathi, S.M. Wood, M.S. Islam, L.F. Nazar, Na-ion mobility in layered Na2FePO4F and olivine Na[Fe,Mn]PO4, Energy Environ. Sci. 6 (2013) 2257. https://doi.org/10.1039/c3ee40914g.
[24] D.D. Yuan, Y.X. Wang, Y.L. Cao, X.P. Ai, H.X. Yang, Improved electrochemical performance of Fe-substituted NaNi0.5Mn0.5O2 cathode materials for sodium-ion batteries, ACS Appl. Mater. Interfaces 7 (2015) 8585–8591. https://doi.org/10.1021/acsami.5b00594.
[25] C.-Y. Yu, J.-S. Park, H.-G. Jung, K.-Y. Chung, D. Aurbach, Y.-K. Sun, S.-T. Myung, NaCrO2 cathode for high-rate sodium-ion batteries, Energy Environ. Sci. 8 (2015) 2019–2026. https://doi.org/10.1039/c5ee00695c.
[26] Y. Jiang, Z. Yang, W. Li, L. Zeng, F. Pan, M. Wang, X. Wei, G. Hu, L. Gu, Y. Yu, Nanoconfined carbon-coated Na3V2(PO4)(3) particles in mesoporous carbon enabling ultralong cycle life for sodium-ion batteries, Adv. Energy Mater. 5 (2015) 1402104. https://doi.org/10.1002/aenm.201402104.
[27] X. Deng, W. Shi, J. Sunarso, M. Liu, Z. Shao, A green route to a Na 2 FePO 4 F-based cathode for sodium ion batteries of high rate and long cycling life, ACS Appl. Mater. Interfaces 9 (2017) 16280–16287. https://doi.org/10.1021/acsami.7b03933.
[28] A. Langrock, Y. Xu, Y. Liu, S. Ehrman, A. Manivannan, C. Wang, Carbon coated hollow Na2FePO4F spheres for Na-ion battery cathodes, J. Power Sources 223 (2013) 62–67. https://doi.org/10.1016/j.jpowsour.2012.09.059.
[29] J. Kim, Y.U. Park, D.H. Seo, J. Kim, S.W. Kim, K. Kang, Mg and Fe Co-doped Mn based olivine cathode material for high power capability, J. Electrochem. Soc. 158 (2011) A250–A254. https://doi.org/10.1149/1.3524260.
[30] M. Yonemura, A. Yamada, Y. Takei, N. Sonoyama, R. Kanno, Comparative kinetic study of olivine LixMPO4 (M = Fe, Mn), J. Electrochem. Soc. 151 (2004) A1352–A1356. https://doi.org/10.1149/1.1773731.
[31] Y.-U. Park, J. Kim, H. Gwon, D.H. Seo, S.W. Kim, K. Kang, Synthesis of multicomponent olivine by a novel mixed transition metal oxalate coprecipitation method and electrochemical characterization, Chem. Mater. 22 (2010) 2573.
[32] C.M. Doherty, R.A. Caruso, B.M. Smarsly, P. Adelhelm, C.J. Drummond, Hierarchically porous monolithic LiFePO4/carbon composite electrode materials for high power lithium ion batteries, Chem. Mater. 21 (2009) 5300–5306. https://doi.org/10.1021/cm9024167.
[33] D. Lepage, C. Michot, G.X. Liang, M. Gauthier, S.B. Schougaard, A soft chemistry approach to coating of LiFePO4 with a conducting polymer, Angew. Chem. Int. Ed. 50 (2011) 6884–6887. https://doi.org/10.1002/anie.201101661.
[34] D.L. Ma, Z.Y. Cao, H.G. Wang, X.L. Huang, L.M. Wang, X.B. Zhang, Three-dimensionally ordered macroporous FeF3 and its in situ homogenous polymerization coating for high energy and power density lithium ion batteries, Energy Environ. Sci. 5 (2012) 8538–8542. https://doi.org/10.1039/c2ee22568a.
[35] A.V. Murugan, T. Muraliganth, A. Manthiram, Rapid microwave-solvothermal synthesis of phospho-olivine nanorods and their coating with a mixed conducting polymer for lithium ion batteries, Electrochem. Commun. 10 (2008) 903–906. https://doi.org/10.1016/j.elecom.2008.04.004.
[36] K.S. Park, S.B. Schougaard, J.B. Goodenough, Conducting-polymer/iron-redox-couple composite cathodes for lithium secondary batteries, Adv. Mater. 19 (2007) 848. https://doi.org/10.1002/adma.200600369.
[37] Y.L. Zhou, Y.L. Li, J. Yang, J. Tian, H.Y. Xu, J. Yang, W.L. Fan, Conductive polymer-coated VS4 submicrospheres as advanced electrode materials in lithium-ion batteries, ACS Appl. Mater. Interfaces 8 (2016) 18797–18805. https://doi.org/10.1021/acsami.6b04444.
[38] F. Wu, J.R. Liu, L. Li, X.X. Zhang, R. Luo, Y.S. Ye, R.J. Chen, Surface modification of Li-rich cathode materials for lithium-ion batteries with a PEDOT:PSS conducting polymer, ACS Appl. Mater. Interfaces 8 (2016) 23095–23104. https://doi.org/10.1021/acsami.6b07431.
[39] T. Ma, Q. Zhao, J.B. Wang, Z. Pan, J. Chen, A sulfur heterocyclic quinone cathode and a multifunctional binder for a high-performance rechargeable lithium-ion battery, Angew. Chem. Int. Ed. 55 (2016) 6428–6432. https://doi.org/10.1002/anie.201601119.

[40] R.V. Apraksin, S.N. Eliseeva, E.G. Tolstopjatova, A.M. Rumyantsev, V.V. Zhdanov, V.V. Kondratiev, High-rate performance of LiFe0.4Mn0.6PO4 cathode materials with poly(3,4-ethylenedioxythiopene):poly(styrene sulfonate)/carboxymethylcellulose, Mater. Lett. 176 (2016) 248–252. https://doi.org/10.1016/j.matlet.2016.04.106.

[41] Y.L. Kuo, C.C. Wu, W.S. Chang, C.R. Yang, H.L. Chou, Study of poly (3,4-ethylenedioxythiophene)/MnO2 as composite cathode materials for aluminum-air battery, Electrochim. Acta 176 (2015) 1324–1331. https://doi.org/10.1016/j.electacta.2015.07.151.

[42] X.L. Fan, C. Luo, J.L. Lamb, Y.J. Zhu, K. Xu, C.S. Wang, PEDOT encapsulated FeOF nanorod cathodes for high energy lithium-ion batteries, Nano Lett. 15 (2015) 7650–7656. https://doi.org/10.1021/acs.nanolett.5b03601.

[43] J. Kim, J.-K. Yoo, Y.S. Jung, K. Kang, Li3V2(PO4)(3)/Conducting polymer as a high power 4 V-class lithium battery electrode, Adv. Energy Mater. 3 (2013) 1004–1007. https://doi.org/10.1002/aenm.201300205.

[44] P.M. Dziewoński, M. Grzeszczuk, Towards TiO2-conducting polymer hybrid materials for lithium ion batteries, Electrochim. Acta 55 (2010) 3336–3347. https://doi.org/https://doi.org/10.1016/j.electacta.2010.01.043.

[45] B.L. Ellis, W.R.M. Makahnouk, W.N. Rowan-Weetaluktuk, D.H. Ryan, L.F. Nazar, Crystal structure and electrochemical properties of A(2)MPO(4)F fluorophosphates (A = Na, Li; M = Fe, Mn, Co, Ni), Chem. Mater. 22 (2010) 1059–1070. https://doi.org/10.1021/cm902023h.

[46] S. Adams, Modelling ion conduction pathways by bond valence pseudopotential maps, Solid State Ionics 136–137 (2000) 1351–1361. https://doi.org/https://doi.org/10.1016/S0167-2738(00)00576-2.

[47] J. Rodríguez-Carvajal, Recent developments of the program FULLPROF, Commission on powder diffraction (IUCr), Newsletter 26 (2001) 12–19.

[48] Y. Lee, J.-K. Yoo, Y. Oh, H. Park, W. Go, S.-T. Myung, J. Kim, Unexpectedly high electrochemical performances of a monoclinic Na2.4V2(PO4)3/conductive polymer composite for Na-ion batteries, J. Mater. Chem. 6 (2018) 17571–17578. https://doi.org/10.1039/c8ta06238b.

[49] W. Ko, T. Park, H. Park, Y. Lee, K.E. Lee, J. Kim, Na0.97KFe(SO4)2: an iron-based sulfate cathode material with outstanding cyclability and power capability for Na-ion batteries, J. Mater. Chem. 6 (2018) 17095–17100. https://doi.org/10.1039/c8ta05854g.

[50] C. Park, S. Im, W. Cho, Y. Kim, J.H. Kim, Facile synthesis of P(EDOT/Ani) : PSS with enhanced heat shielding efficiency via two-stage shot growth, RSC Adv. 8 (2018) 12992–12998. https://doi.org/10.1039/c8ra01122b.